

# Dynamical evolution of V-type asteroids in the central main belt

V. Carruba<sup>1\*</sup>, M. E. Huaman<sup>1</sup>, R. C. Domingos<sup>2,1</sup>, C. R. Dos Santos<sup>1</sup>, and D. Souami<sup>3,4,5</sup>

<sup>1</sup>UNESP, Univ. Estadual Paulista, Grupo de dinâmica Orbital e Planetologia, Guaratinguetá, SP, 12516-410, Brazil

<sup>2</sup>INPE, Instituto Nacional de Pesquisas Espaciais, So Jos dos Campos, SP, 12227-010, Brazil

<sup>3</sup>NAXYS, Namur Center for Complex Systems, Department of Mathematics, University of Namur, 5000 Namur, Belgium

<sup>4</sup>UPMC, Université Pierre et Marie Curie, 4 Place Jussieu, 75005, Paris, France

<sup>5</sup>SYRTE, Observatoire de Paris, Systèmes de Référence Temps Espace, CNRS/UMR 8630, UPMC, Paris, France;

Accepted 2014 January 24. Received 2014 January 23; in original form 2013 December 9

## ABSTRACT

V-type asteroids are associated with basaltic composition, and are supposed to be fragments of crust of differentiated objects. Most V-type asteroids in the main belt are found in the inner main belt, and are either current members of the Vesta dynamical family (Vestoids), or past members that drifted away. However, several V-type photometric candidates have been recently identified in the central and outer main belt.

The origin of this large population of V-type objects is not well understood. Since it seems unlikely that Vestoids crossing the 3J:-1A mean-motion resonance with Jupiter could account for the whole population of V-type asteroids in the central and outer main belt, origin from local sources, such as the parent bodies of the Eunomia, and of the Merxia and Agnia asteroid families, has been proposed as an alternative mechanism.

In this work we investigated the dynamical evolution of the V-type photometric candidates in the central main belt, under the effect of gravitational and non-gravitational forces. Our results show that dynamical evolution from the parent bodies of the Eunomia and Merxia/Agnia families on timescales of 2 Byr or more could be responsible for the current orbital location of most of the low-inclined V-type asteroids.

**Key words:** Minor planets, asteroids: general – Minor planets, asteroids: classes: V-types – celestial mechanics.

## 1 INTRODUCTION

The V-type asteroids, which are characterized by 1 and 2  $\mu\text{m}$  absorption bands in the infrared spectrum, are associated with basaltic composition, and are supposed to be fragments of the crust of differentiated objects. Most of the V-type asteroids in the main belt are found in the inner main belt (defined as the region in semi-major axis between the 4J:-1A and 3J:-1A mean-motion resonances with Jupiter), and are either members of the dynamical Vesta family (Vestoids), or are thought to be past members that dynamically migrated beyond the limits of the current Vesta family. Recently, two new basaltic asteroids, (1459) Magnya (Lazzaro et al. 2000), and (10537) (1991 RY16) (Moskovitz et al. 2008b), were identified in the outer main belt (the region between the 5J:-2A and 2J:-1A mean-motion resonances), a region too far away from Vesta to possibly be dynamically connected

with this asteroid. Roig and Gil-Hutton (2006) used Sloan Digital Sky Survey-Moving Object Catalog data, fourth release (SDSS-MOC4) multi-band photometry to infer the asteroid taxonomy, and identified several V-type photometric candidates in the central (defined as the region between the 3J:-1A and 5J:-2A mean-motion resonances) and outer main belt. Most recently, Carvano et al. (2010) identified hundreds of photometric candidates in the central and outer main belt. Roig et al. (2008) discussed the possibility that some of these asteroids could be former Vestoids that crossed the 3J:-1A mean-motion resonance with Jupiter, but this mechanism alone seems to be unlikely to have produced the whole observed population of V-type candidates, especially those in the outer part of the central main belt.

Alternative production mechanisms have therefore been suggested to explain the presence of these objects. Carruba et al. (2007a) suggested that three V-type asteroids in the central main belt, (21238), (40621) and (66905) could have originated as fragments of the crust of the parent body of

\* E-mail: vcarruba@feg.unesp.br

the Eunomia family, that, according to Nathues et al. (2005) might have been a differentiated or partially differentiated body. This mechanism may have originated some of the basaltic material in the central main belt. However, since the work of Carvano et al. (2010) identified more than one hundred V-type photometric candidates in the central main belt, and since some of these objects have very different values of inclination with respect to (15) Eunomia, yet another mechanism to produce basaltic material may have been at work.

Luckily, other possible sources of basaltic material were identified in the central main belt by other authors. Observations of (808) Merxia and (847) Agnia by Sunshine et al. (2004) showed that the spectra of both these objects are compatible with an S-type asteroid with both low and high calcium forms of pyroxene on the surface, along with less than 20% olivine. The high-calcium form of pyroxene forms 40% or more of the total pyroxene present, indicating a history of igneous rock deposits. This suggested that the asteroids underwent differentiation by melting, creating a surface of basalt rock.

The members of these families, including their namesakes, according to Sunshine et al. (2004), most likely formed from the breakup of a basalt object, which in turn was spawned from a larger parent body that had previously undergone igneous differentiation. Since the Merxia and Agnia families have lower values of inclinations than (15) Eunomia, could it be possible that some of the V-type photometric candidates currently at low- $i$  may have originated from the parent body of these two families?

In this work we will investigate possible paths of diffusion from the current orbital location of the photometric candidates in the central main belt, in order to infer possible clues on their origin. Since Moskovitz et al. (2008a) suggested that it was not likely to have had hundreds of differentiated bodies in the primordial main belt, but that the number was more likely of the order of dozens, we will try to assess how much a model with two sources in the central main belt, the parent bodies of the Eunomia and that of the Merxia/Agnia families, may succeed or not in reproducing the current distribution of V-type photometric candidates.

This paper is so divided: in Sect. 2 we discussed the current knowledge on V-type photometric candidates in the central main belt, obtained in previous works (Roig and Gilhutton 2006, Carvano et al. 2010, De Sanctis et al. 2011) and by our group using the approach of DeMeo and Carry (2013). Five different orbital regions characterized by the presence of basaltic material are introduced in this section. In Sect. 3 we discuss the groups identified in Sect. 2 in terms of ejection velocities with respect to Eunomia, diameters, geometrical albedos, and masses. In Sect. 4 we study the local web of mean-motion and secular resonances using dynamical maps of synthetic proper elements. In Sect. 5 we analyze how dynamical evolution caused by the Yarkovsky effect may have caused the current orbital distribution of V-type asteroids, and in Sect. 6 we study the long-term effects of close encounters with massive asteroids in the central main belt. Finally, in Sect. 7 we present our conclusions.

## 2 IDENTIFICATION: SPECTRAL TAXONOMY AND SDSS-MOC4 DATA

Carvano et al. (2010) studied the taxonomy of asteroids observed by the Sloan Digital Sky Survey-Moving Object Catalog data, fourth release (SDSS-MOC4 hereafter, Ivezić et al. 2001). This survey provided a sample two order of magnitude larger than any available in any current spectroscopic catalogs (about 60000 numbered objects). The authors identified 130 V-type photometric candidates in the central main belt, including QV, SV objects, and other dubious cases, in the central main belt, based on a taxonomical scheme in the plane of  $(a^*, i - z)$  colors, and posted their results on the Planetary Data System, available at <http://sbn.psi.edu/pds/resource/sdsstax.html>, and accessed on September 10<sup>th</sup> 2013.

DeMeo and Carry (2013) recently introduced a new classification method, based on the Bus-DeMeo taxonomic system, that employs SDSS-MOC4 gri slope and  $z' - i'$  colors. In that article the authors used the photometric data obtained in the five filters  $u', g', r', i',$  and  $z'$ , from 0.3 to 1.0  $m$ , to obtain values of  $z' - i'$  colors and spectral slopes over the  $g', r',$  and  $i'$  reflectance values. Values of  $z' - i'$  colors and spectral slopes were then used to assess if an asteroid belonged to a given spectral class, whose boundary values were determined in this domain by the authors. For overlapping classes, the taxonomy is assigned in the last class in which the object resides, in the following order: C-, B-, S-, L-, X-, D-, K-, Q-, V-, and A-types. Since some asteroids had multiple observations in the SDSS-MOC4 database, we adopted the DeMeo and Carry (2013) criteria for classifications in these cases: in case of conflicts, the class with the majority number of classifications is assigned.

With respect to the work of Carvano, we identified six new photometric candidates in the central main belt, and eleven in the outer main belt. Table 1 displays our new results. All V-type photometric candidates identified by Carvano et al. (2010) are also listed in Table 3. We report the asteroid identification, if it is a confirmed V-type object, the asteroid proper elements  $a, e,$  and  $\sin(i)$ , the absolute magnitude ( $H$ ), the diameter ( $D$ ), and geometric albedo ( $p_V$ ), according to the WISE mission, when available. The asteroid (177904) (2005 SV5) was already identified as a possible V-type photometric candidate in Carruba et al. (2013b). Being this a paper centered on the dynamical evolution of V-type candidates in the central main belt only, asteroids in the outer main belt are only given as a reference to the observing community,

We selected all asteroids in the Carvano et al. (2010) database, available in the the Planetary Data System, and in the HORIZONS system of the Jet Propulsion laboratory <sup>1</sup>, that were V-type photometric candidates (including SV and QV types), had proper elements as reported by the AstDyS site <http://hamilton.dm.unipi.it/cgi-bin/astdys/astibo>, (accessed on September 15<sup>th</sup>, 2013, Knežević and Milani 2003), and had orbits in the central main belt, defined as  $a_{31} < a < a_{52}$ , where  $a_{31}$  and  $a_{52}$  are the semi-major axis of the center of the 3J:-1A and 5J:-2A mean motion resonances with Jupiter, respectively. Overall, including the new photometric candidates identified in this work, we encountered 255

<sup>1</sup> The Database was accessed on September 13<sup>th</sup> 2013.

**Table 1. List of new V-type photometric candidates in the central and outer Main-belt.**

Asteroid Id.	Spectral type	$a$	$e$	$\sin(i)$	$H$	$D$ (km)	$p_v$
7472	V?	3.010245	0.138886	0.156293	12.08	10.008	0.2795
11465	V?	3.102607	0.014941	0.348060	12.87	12.556	0.0775
18802	V?	2.687340	0.143116	0.215531	13.82	3.940	0.3134
35567	V	2.567894	0.089490	0.196503	14.58	2.381	0.4504
55270	V	2.908541	0.125003	0.164700	14.02		
57322	V?	2.584340	0.164743	0.130332	14.86		
88084	V?	2.545195	0.152695	0.088088	15.30		
91159	V	3.194682	0.273886	0.277364	14.28		
92182	V?	3.181359	0.169964	0.266076	13.70		
93981	V	2.662526	0.019289	0.226328	13.85	3.376	0.4268
177904	V	3.158618	0.153963	0.073138	15.30	5.762	0.0403
208324	V	3.130781	0.270397	0.287020	14.91		
217953	V?	2.546619	0.162840	0.176317	16.37		

V-type candidates, of which 127 are pure V-types (excluding SV, QV, and other dubious cases), and objects, (21238), (40521), and (66905) are confirmed V-type asteroids whose spectra were obtained in De Sanctis et al. (2011). Our results are shown in Fig. 1, where we display a proper  $(a, e)$  (panel A) and  $(a, \sin(i))$  projections of the proper elements of all candidates (blue dots), of pure V-type candidates (green full dots) and of the confirmed V-type asteroids (red full dots). Vertical lines identify the location of the main local mean-motion resonances, blue lines show the position of the center of secular resonances, computed using the analytical theory of Milani and Knežević (1994) to compute the proper frequencies  $g$  and  $s$  for the grid of  $(a, e)$  and  $(a, \sin(i))$  values shown in Fig. 1 and the values of angles and eccentricity of (480) Hansa, the asteroid with the largest family in the highly inclined region. In panel A, we also display the lines for which  $q = Q_{Mars}$ , and  $q = q_{Mars}$ , where close encounters with terrestrial planets start to be possible.

One may notice six regions of concentrations of V-type candidates in the  $(a, \sin(i))$  plane: one region around the Eunomia family, in the inner central main belt ( $a_{31} < a < a_{83}$ ), that includes the three confirmed V-type asteroids discussed in Carruba et al. (2009), at intermediate values of  $\sin(i)$  ( $0.12 < \sin(i) < 0.3$ ). A concentration of asteroids near the Astraea family, in the inner central main belt, at low inclinations ( $\sin(i) < 0.12$ ). Eight asteroids in the highly inclined region ( $\sin(i) > 0.3$ ), mostly found in the Hansa family region. Finally, three alignments of asteroids (possibly four, if we include less than “pure” V-type candidates), in the outer central main belt ( $a_{83} < a < a_{52}$ ), in the regions of the Merxia-Agnia, Gefion, and (1995 SU37) asteroid families, with values of  $\sin(i)$  lower than 0.12 (Lavrov),  $0.12 < \sin(i) < 0.19$  (Gefion), and  $\sin(i) > 0.19$ , respectively. We define these regions as Hansa, Eunomia, Astraea, Merxia, and Gefion<sup>2</sup>, and assign each V-type candidate to its own region, whose boundaries are shown in Fig. 1, panel B. Results are also listed in Table 3. We also checked how many of the known “pure” V-type candidates are members of known asteroid families, according to the AstDyS site. We found 22 asteroids belonging to a family, most of which

(six, 27.27% of the total) members of the Eunomia family, followed by four objects (18.18%) in the Hansa family. Of the remaining asteroids belonging to identified families, two were in the Juno family, one in the Minerva group, one in the 11882 (1990 RA3), one in the Maria family (all groups near the Eunomia orbital region), one was in the Astraea family, and the remaining asteroids were found in families in the outer central main belt, including one in the Merxia family. The fact that the majority of V-type candidates belonging to a family are to be found in the orbital region of the Eunomia asteroid family may be an indirect confirmation of the role that the parent body of this family may have played as a source of V-type asteroids in the central main belt (Carruba et al. 2009).

To numerically check for the statistical significance of the Eunomia and Merxia/Agnia parent bodies as sources of basaltic material in the central main belt, we performed this numerical experiment: following the approach of Carruba and Machuca (2011), we estimated the probability that a number of objects be produced by a Poisson distribution assuming that the expected number of  $k$  occurrence in a given interval is given by:

$$f(k, \lambda) = \frac{\lambda^k e^{-\lambda}}{k!}, \quad (1)$$

where  $\lambda$  is a positive real number, equal to the expected number of occurrences in the given interval. For our purposes we used for  $\lambda$  the mean values of objects expected in the regions of the halos of the Eunomia and Merxia/Agnia families<sup>3</sup>. This is given by the equation:

$$\lambda = N_{ast} \cdot \frac{V_{halo}}{V_{Tot}} \quad (2)$$

where  $N_{ast}$  is the total number of V-type photometric candidates,  $V_{halo}$  is the volume in the  $(a, e, \sin(i))$  space occupied by the family halo and  $V_{Tot}$  is the total volume occupied by all photometric candidates, defined as the region between

<sup>3</sup> We did not perform a statistical analysis of the region of Hansa, because this family is in a stable island located between the 3J-1A and 8J-3A mean-motion resonances in proper  $a$ , and between the  $\nu_6$  and  $\nu_5$  secular resonance in  $\sin(i)$  (Carruba 2010b). While 80% of the highly inclined V-type photometric candidates are members of this family this may not be statistically significant because of the local dynamics.

<sup>2</sup> We consider the two alignments in the regions of the Gefion and (1995 SU37) asteroid families to be part of the same “Gefion” region.

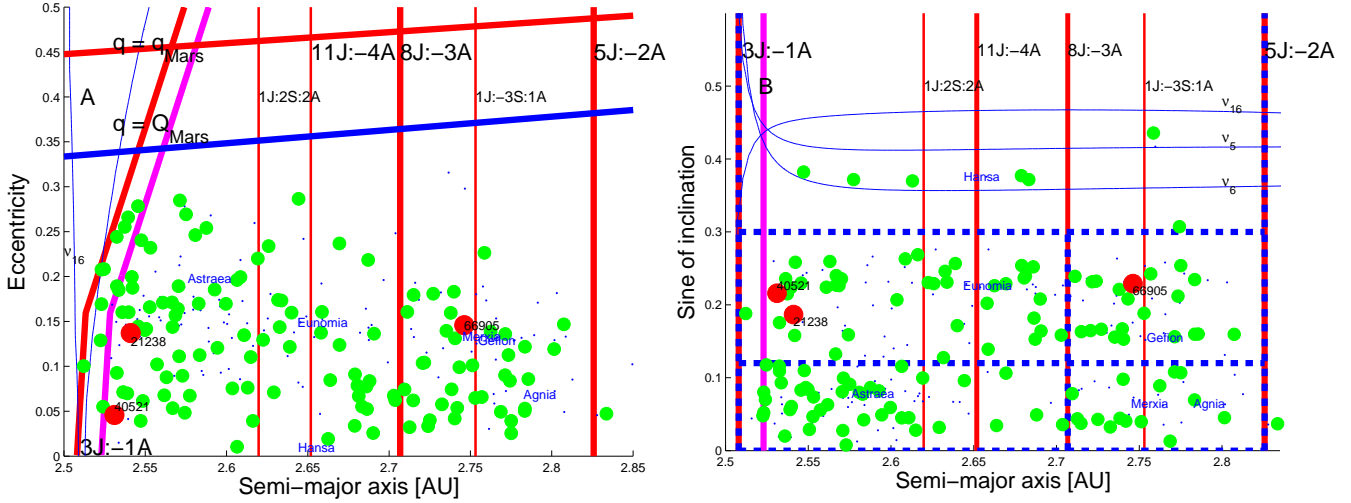


**Figure 1.** Panel A: Semi-major axis versus eccentricity of the V-type candidates identified using SDSS-MOC4 in the central main belt. Blue dots identified the orbital location of all photometric candidates, green full dots are associated with “pure” V-type candidates, and confirmed V-types are shown as red full dots. Vertical red lines display the location of mean-motion resonances, and blue lines show the center of secular resonances (see text for details). The magenta line is associated with the unstable region (on timescales of 100 Myr) near the 3J:-1A mean-motion resonance, as identified by Guillens *et al.* (2002). Finally, we also display the lines for which  $q = Q_{Mars}$ , and  $q = q_{Mars}$ , where close encounters with terrestrial planets start to be possible. Panel B: Semi-major axis versus sine of proper inclination of the same V-type candidates. Blue dotted lines identify the boundaries of the regions discussed in the text.

the 3J:-1A and 5J:-2A mean motion resonances with Jupiter in semi-major axis (i.e.,  $2.508 < a < 2.826$  AU), and eccentricity and  $\sin(i)$  from zero to the maximum value of any V-type candidate in the central main belt (0.2865 and 0.3822, respectively). For the volume of the Eunomia family halo we used a simple parallelepipedal defined according to the maximum values of  $(a, e, \sin(i))$  observed for the Eunomia family core and halo as found in Carruba *et al.* (2007a):  $2.508 < a < 2.707$  AU,  $0.12 < e < 0.16$ ,  $0.18 < \sin(i) < 0.24$  (Eunomia core), and  $2.508 < a < 2.753$  AU,  $0.12 < e < 0.19$ ,  $0.18 < \sin(i) < 0.26$  (Eunomia halo). Since we have no information on the possible extent of the proto-family that originated the Merxia and Agnia families, in this case we used as boundaries the combined limits of the halos of the two families in the  $(a, e, \sin(i))$  space, as determined by Carruba *et al.* (2013b):  $2.707 < a < 2.826$ ,  $e < 0.15$ , and  $\sin(i) < 0.12$ .

Using standard statistical terminology, we define the null hypothesis as the possibility that the data are drawn from a given distribution. We can reject the null hypothesis if it is associated with a probability lower than a threshold, usually of the order of 1%. Using Eq. 1, we found that the probability that the 6 asteroids in the Eunomia core region, 15 asteroids in the Eunomia halo region, and the 15 found in the Merxia/Agnia halo region could be explained as fluctuations of a Poissonian distribution are of  $7.0 \cdot 10^{-3}$ ,  $1.7 \cdot 10^{-4}$  and  $8.1 \cdot 10^{-3}$ , i.e., below the null hypothesis threshold ( $1.0 \cdot 10^{-2}$ ). A similar analysis done for the uniform and Gaussian distributions, according to the procedure described in Carruba and Machuca (2011), also provided values of probabilities below the null hypothesis, so suggesting that the higher density of objects found in the Eunomia and Merxia/Agnia regions may be caused by a possible local source.

Finally, since these 1-dimensional statistical analysis are somewhat dependent on the choice of the regions bound-

aries, we also performed Mardia’s test (Mardia 1970) on multivariate normality for the whole 128 asteroid population. We assume that the distribution in the  $(a, e, \sin(i))$  domain has a tri-variate Gaussian probability density function given by:

$$f(\mathbf{x}) = \frac{1}{(2\pi)^{3/2} \sqrt{|\Sigma|}} \exp\left(-\frac{1}{2}(\mathbf{x} - \mu)' \Sigma^{-1}(\mathbf{x} - \mu)\right), \quad (3)$$

where  $\mathbf{x}$  is the vector  $(a, e, \sin(i))$ ,  $\mu$  is the vector with components equal to the mean values of  $a$ ,  $e$  and  $\sin i$  of the observed population, and  $\Sigma$  is the covariance matrix, that can be estimated numerically having  $n$   $x_j$  vectors using the equation:

$$\Sigma = \frac{1}{n} \sum_{j=1}^n (\mathbf{x}_j - \mu) \cdot (\mathbf{x}_j - \mu)^T, \quad (4)$$

Mardia’s test is based on multivariate extensions of skewness and kurtosis measures. For a sample  $(x_1, \dots, x_n)$  of  $p$ -dimensional vectors we can compute the A and B parameters given by:

$$A = \frac{1}{6n} \sum_{i=1}^n \sum_{j=1}^n [(\mathbf{x}_i - \mu)^T \Sigma^{-1}(\mathbf{x}_j - \mu)]^3, \quad (5)$$

and

$$B = \frac{\sqrt{n}}{\sqrt{8p(p+2)}} \left[ \frac{1}{n} \sum_{i=1}^n [(\mathbf{x}_i - \mu)^T \Sigma^{-1}(\mathbf{x}_i - \mu)]^2 - p(p+2) \right], \quad (6)$$

where  $\Sigma^{-1}$  is the inverse of the covariance matrix given by Eq. 4. Under the null hypothesis of multivariate normality, the statistic  $A$  will have approximately a chi-squared distribution with  $\frac{1}{6}p(p+1)(p+2)$  degrees of freedom (10 for  $p=3$ ), and  $B$  will be approximately standard normal with mean zero and standard deviation one. We computed  $A$  and  $B$  for our sample of 128 asteroids and we obtained

$A = 27.389$  and  $B = 1.7 \cdot 10^3$ , that have probabilities of being associated with a  $\chi^2$  and a normal distribution lower than  $4.5 \cdot 10^{-5}$ . We can therefore safely assume that V-type photometric candidates do not follow a tri-variate Gaussian distribution as a whole.

In the next section we will further analyze the six dynamical regions defined in this section.

### 3 GROUPS OF V-TYPE CANDIDATES AND THEIR POSSIBLE ORIGIN

First, to test for the reality of the six concentration groups identified in Sect. 2 we performed the following numerical experiment: we computed the distances with respect to (15) Eunomia according to the distance metrics (Zappalá et al. 1995)<sup>4</sup>:

$$d = na\sqrt{h_1\left(\frac{\Delta a}{a}\right)^2 + h_2(\Delta e)^2 + h_3(\Delta(\sin(i)))^2}, \quad (7)$$

where  $n$  is the asteroid proper motion,  $a$ ,  $e$ , and  $\sin(i)$  are the standard set of proper elements (semi-major axis, eccentricity, and sine of the inclination), and  $h_i$  ( $i=1,2,3$ ) are numerical constants equal to  $5/4$ ,  $2$ , and  $2$  for the standard metric of Zappalá et al. (1995). Other choices of the  $h_i$  constants are possible and discussed in the literature (see also Carruba and Michtchenko 2007). The advantage of using distances  $d$  rather than bidimensional plots as those shown in Fig. 1 is that these quantities account for distances in a three-dimensional space and are not subjected to the distortions that arise from plotting three dimensional distributions in two-dimensional spaces.

Fig. 2, panel A, displays an  $(a, \sin(i))$  plot of V-type photometric candidates in the central main belt. Distances in proper element domains of V-type asteroids in the central main belt with respect to (15) Eunomia are plotted with this color code: red full dots identify objects with  $d < 1000$  m/s, yellow full dots asteroids with  $1000 < d < 3000$  m/s, and green dots bodies with  $d > 3000$  m/s. The other symbols are the same as in Fig. 1. Objects nearest to the Eunomia family (red and yellow dots) correspond to the Eunomia family region and the two horizontal “strips” in the outer central main belt at  $\sin(i) > 0.12$  defined in Sect. 2. Green asteroids are found in the “Astraea” region, in the  $\sin(i) < 0.12$  outer central main belt strip, and in the highly inclined region. With the exception of seven objects, we confirm the  $0.12 < \sin(i) < 0.3$  criteria for asteroids possibly originating from the Eunomia family defined in Sect. 2.

We also computed distances with respect to the Merxia “region”. Since the original orbital parameters of the possible parent body of the Merxia and Agnia families are unknown, we computed distances with respect to the largest surviving fragment, (808) Merxia itself. Our results are shown in Fig. 2, panel B. Low-inclined objects have smaller

<sup>4</sup> We should point out that these distances, while expressed in m/s, are not exactly ejection velocities, that should be computed using Gauss equation (see also Carruba et al. 2003). Since, however, ejection velocities computed with such an approach also depend on the unknown true anomaly and argument of pericenter at the moment of impact of the parent body, in this work we prefer to use this simpler approach.

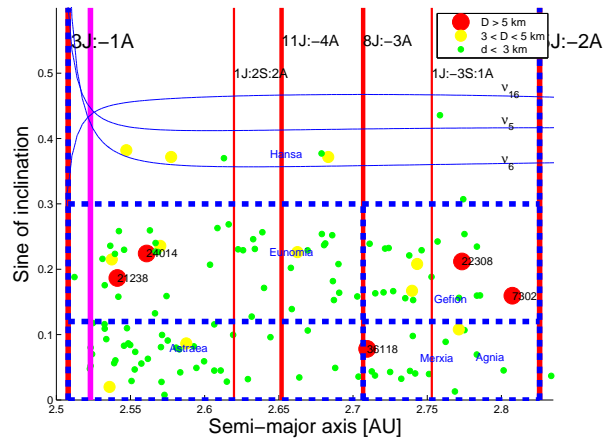


**Figure 3.** An  $(a, \sin(i))$  projection of V-type photometric candidates in the central main belt. The size of the symbol is associated with the asteroid diameter, according to the figure legend. The other symbols have the same meaning as those in Fig. 1, panel B.

distances with respect to Merxia than Eunomia. The strip of aligned asteroids in the Gefion region, that was found to be at relatively low distances from (15) Eunomia, appears to be within reach of (808) Merxia as well, which suggests that either sources could be responsible for these asteroids. Overall, these results seem to suggest a second possible source of basaltic material in the central main belt.

We then turned our attention to the diameters of photometric V-type candidates in the central main belt. Results from the Wide-field Infrared Survey Explorer (WISE) (Wright et al. 2010), and the NEOWISE (Mainzer et al. 2011) enhancement to the WISE mission recently allowed to obtain diameters and geometric albedo values for more than 100,000 Main Belt asteroids (Masiero et al. 2011). Of the 127 V-type candidates in the central main belt, 27 had values of diameters and geometric albedos listed in the WISE dataset. Concerning the other asteroids, their diameters and albedos can be estimated using the relationship (Harris and Lagerros 2002):

$$D = \frac{1329km}{\sqrt{p_V}} \cdot 10^{-H/5}, \quad (8)$$

For the objects lacking WISE albedo data, we used the mean value of the albedo available for the other 27 bodies, i.e.,  $p_V = 0.238$ . The minimum value of albedo was of 0.0518, and the maximum of 0.4268. Each of the extreme values of  $p_V$  was only reached once, and if we eliminate such outliers from the mean, we obtained a mean value of 0.2379, very close to the mean value obtained with the outliers.

Fig. 3 displays an  $(a, \sin(i))$  projection of V-type photometric candidates in the central main belt. The size of the symbol is associated with the asteroid estimated diameter: large full red dot display the orbital position of the five objects with  $D > 5$  km, yellow full dots show the position of the asteroids with  $3 < D < 5$  km, and the green dots are associated with smaller bodies. One can notice that, with the exception of the asteroid (36118), that is barely 5 km in diameter, all larger objects are found at  $\sin(i) > 0.12$ . Only two medium-sized asteroids are encountered in the “Astraea” region.

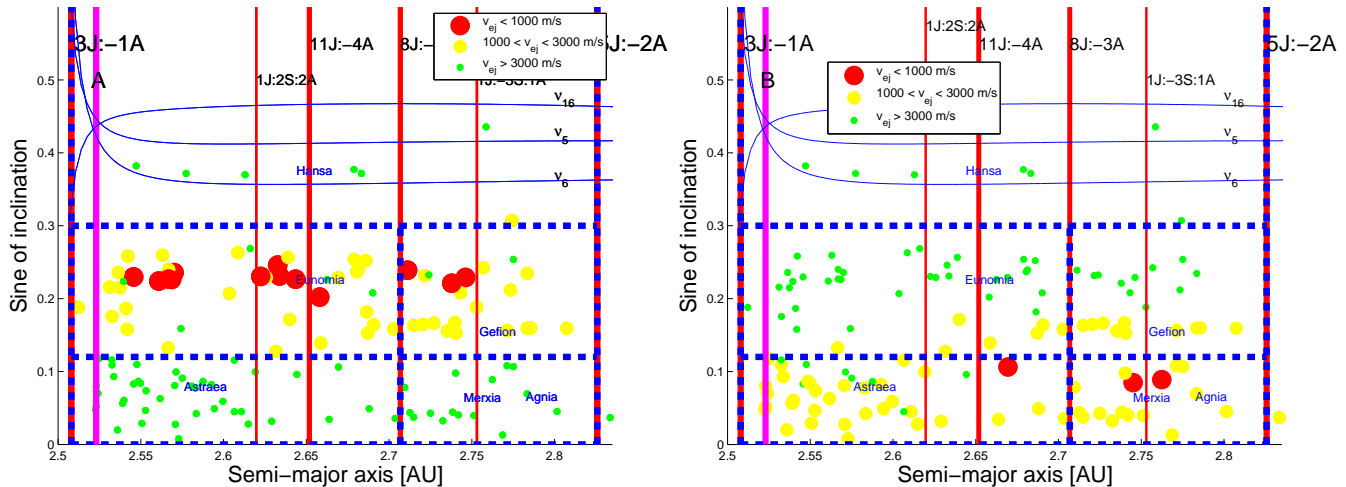


**Figure 2.** An  $(a, \sin(i))$  plot of V-type photometric candidates in the central main belt. Distances in proper element domains of V-type asteroids in the central main belt with respect to (15) Eunomia are plotted with this color code: red full dots identify objects with  $d < 1000$  m/s, yellow full dots asteroids with  $1000 < d < 3000$  m/s, and green dots bodies with  $d > 3000$  m/s. The other symbols have the same meaning as those in Fig. 1, panel B.

To estimate how much mass is contained in the currently known V-type candidates in the central main belt we estimated the mass of each object using the equation (Moskovitz et al. 2008a, eq. 6):

$$M(H) = (1.28 \cdot 10^{18} \text{ kg}) \frac{\rho}{pv^{3/2}} 10^{-0.6H}, \quad (9)$$

where  $\rho$  is the bulk density, assumed equal to  $3000 \text{ kg/m}^3$  for V-type objects, and asteroids have been assumed to be spherical bodies. Using the values of geometrical albedo  $pv$  previously discussed in this section, we obtain a total mass of  $1.81 \cdot 10^{15} \text{ kg}$ , which is just 0.139% of the estimated mass escavated from craters in Vesta  $1.3 \cdot 10^{18} \text{ kg}$  (Moskovitz et al. 2008a). Only a very minor fraction of the basaltic material present in the main belt is therefore located in the central main belt. In the next section we will discuss how the V-type photometric candidates are located with respect to the local web of mean-motion and secular resonances.

#### 4 DYNAMICAL MAPS

To investigate in further detail the local dynamics we computed a dynamical map of synthetic proper elements with 19800 test particles in the region of the central main belt. We used the SWIFT\_MVFS symplectic integrator from the SWIFT package (Levison and Duncan, 1994) modified by Brož (1999) so as to include on-line digital filtering to remove all frequencies with periods less than 600 yr. We used a step in  $a$  of 0.005 AU and in  $i$  of  $0.2^\circ$ , and took particles in an equally spaced grid of 165 by 120 particles in the  $(a, \sin(i))$  plane, the representative plane for studying diffusion of members of asteroid families<sup>5</sup>. The initial values of  $e, \Omega, \omega$ , and  $\lambda$  of the test particles were fixed at

<sup>5</sup> Our particles covered a range between 2.5 and 2.828 AU in  $a$ , and  $0^\circ$  and  $23.8^\circ$  in  $i$ , respectively. Since the local dynamics has been studied in detail in several other works, (see also Carruba et al. 2007b), and since the proper eccentricity of asteroid is changed

those of (15) Eunomia, the largest member of its family and a possible source of V-type asteroids, according to Carruba et al. (2007b). We computed synthetic proper elements  $(a, e, \sin(i))$  and frequencies  $(n, g, s)$  of these test particles with the approach described in Carruba (2010).

Results are shown in Fig. 4. Black dots identify the orbital position in the plane of proper  $(a, \sin(i))$  of each simulated test particle. Unstable regions will appear as devoided of test particles, mean-motion resonances will show as vertical alignments, and secular resonances will be associated with inclined alignments of dots. In color we show test particles whose frequency values where within  $\pm 0.3 \text{ arcsec/yr}$ <sup>6</sup> from the center of the  $z_1 = \nu_6 + \nu_{16} = g - g_6 + s - s_6$  (magenta dots), the  $2\nu_6 - \nu_5 = g + g_5 - 2g_6$  (yellow dots), and from the  $\nu_5 - \nu_6 + \nu_{16} = g + g_5 - 2g_6$  (orange dots) resonances, respectively. The other symbols are the same as in Fig. 1. While all the other secular resonances up to order six present in the region were studied, we choose to display in the figure the orbital location of these three resonances only because of their dynamical importance. The  $z_1$  secular resonance played a major role in the dynamical evolution of the Agnia (Vokhrouhlický et al. 2006) and Padua (Carruba 2009a) families, that are characterized by the fact that the majority of their members are in librating states of this resonances. The  $z_1$  conserved quantity allowed to obtain better estimates of the extent of the original ejection velocity field of these two families. The  $2\nu_6 - \nu_5$  had one of the largest population of likely resonators in our dynamical map, and its possible role in the dynamical evolution of V-type photometric candidates will be further investigated in this section.

more easily than its proper inclination, we did not performed in this work analysis in the  $(a, e)$  and  $(e, \sin(i))$  planes.

<sup>6</sup> The so-called likely resonators, or objects with a probability higher than 90% of being in librating states of the resonances, as defined in Carruba (2009a). Likely resonators are found by equating the values of the asteroidal frequencies to the planetary ones. In the case of the  $z_1$  secular resonance, we have  $g - g_6 + s - s_6 \simeq 0$ , which implies  $g + s = g_6 + s_6 = 1.898 \text{ arcsec/yr}$ .

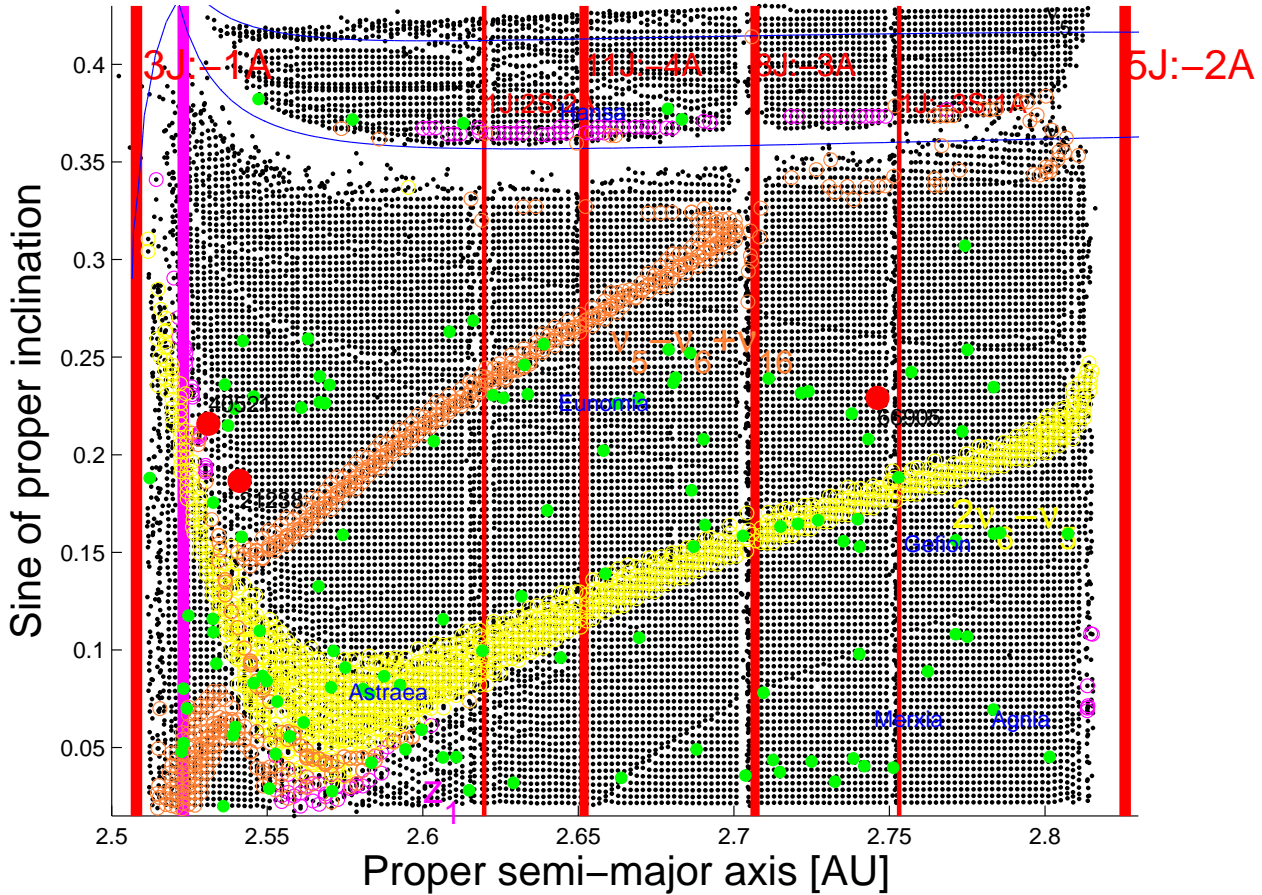


**Figure 4.** An  $(a, \sin(i))$  proper element map of the central main belt. Black dots identify the orbital position in the plane of proper  $(a, \sin(i))$  of each simulated test particle. Color circles are associated with asteroids likely to be in secular resonance configurations, according to the color code described in the text. The other symbols have the same meaning as in Fig. 1.

Finally, the  $\nu_5 - \nu_6 + \nu_{16}$  secular resonance was shown to be one possible mechanism of delivery of basaltic material from the Eunomia family to lower inclination regions in Carruba et al. (2007a). Its dynamical importance will also be discussed in Sect. 5.

Other minor secular resonances were identified in the dynamical map, but were not shown for simplicity. The Eunomia and Gefion regions are crossed by the  $3\nu_6 - \nu_5$  and  $z_2 = 2\nu_6 + \nu_{16} = 2(g - g_6) + s - s_6$  non-linear secular resonances. The  $2\nu_6 + \nu_{17} = 2(g - g_6) + s - s_7$  secular resonance is present in the Merxia region. Finally, the Hansa region is crossed by the  $\nu_5 + 2\nu_{16} = g - g_5 + 2(s - s_6)$ ,  $\nu_6 - \nu_{16} = g - g_6 - s + s_6$ , and  $\nu_5 - \nu_{16} = g - g_5 - s + s_6$ , secular resonances (see also Carruba 2010). The last entry of Table 3 identifies asteroids that are likely resonators of the discussed secular resonances. Incidentally, there are three objects (93620, 108901, 225791) that are likely resonators of two resonances at the same time, i.e., they are at the crossing of two secular resonances.

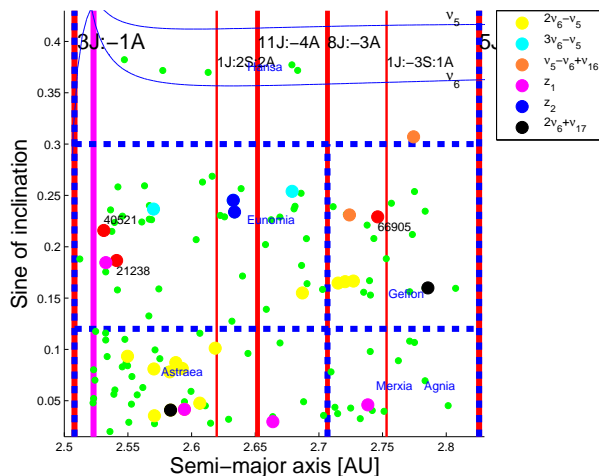
To understand the importance of secular dynamics for the evolution of V-type asteroids in the central main belt, we also selected “likely resonators” among the photometric V-type candidates. Our results are listed in Table 2, that

displays the name of the resonance, its type, i.e., what asteroidal frequencies are involved, the resonance center as previously defined in this section, and the number of likely resonators for the resonances that had at least one librating candidate. An  $(a, \sin(i))$  projection of the identified likely resonators is also shown in Fig. 5.

The largest population of likely resonators is found in the  $2\nu_6 - \nu_5$  secular resonance, with 15 candidates. All the other resonances had four resonators or less. The relatively large number of candidates in this  $g$ -type resonance may have interesting repercussions on the dynamics of V-type asteroids. One may wonder if the cluster of V-type asteroids in the Astraea region may be caused by an accumulation of asteroids in this region. To start answering this question, following the approach of Carruba et al. (2013b) we integrated the likely resonators in the  $2\nu_6 - \nu_5$  secular resonances for 10 Myr under the influence of all planets, and checked the behavior of the resonant argument. 11 asteroids are in librating states, 2 in circulating states, and 2 are alternating phases of circulation and libration. The large fraction of actual resonators among the candidates suggest that this is indeed a powerful resonance. Its role when the Yarkovsky force is considered will be discussed in Sect. 5, but, being a

**Table 2.** Likely resonators among V-type photometric candidates.

Resonant name	Type	Resonant center [arcsec/yr]	# of likely resonators
$2\nu_6 - \nu_5$	$g$	52.229	15
$3\nu_6 - \nu_5$	$g$	40.236	3
$\nu_5 - \nu_6 + \nu_{16}$	$s$	-50.300	2
$\nu_6 + \nu_{16} = z_1$	$g + s$	1.998	4
$2\nu_6 + \nu_{16} = z_2$	$2g + s$	30.141	2
$2\nu_6 + \nu_{17}$	$2g + s$	53.141	2

**Figure 5.** Projection in the proper  $(a, \sin(i))$  plane of the likely resonators population (colored circles) listed in Table 2, according to the color code displayed in the figure legend.

pericenter resonance, it seems unlikely that it will be able to significantly change the inclination of wandering asteroids. In the next section we will try to answer this and other questions on the possible origin of photometric V-type asteroids in the central main belt.

## 5 YARKOVSKY EVOLUTION

To investigate the dynamical evolution of V-type candidates in the central main belt, we integrated clones of these objects with SWIFT-RMVSY, the symplectic integrator of Brož (1999) that simulates the diurnal and seasonal versions of the Yarkovsky effect, over 30 Myr and the gravitational influence of all planets from Venus to Neptune (Mercury was accounted for as a barycentric correction in the initial conditions). We used values of the Yarkovsky parameters appropriate for V-type asteroids: a thermal conductivity  $K = 0.001 \text{ W/m/K}$ , a thermal capacity  $C = 680 \text{ J/kg/K}$ , surface density  $1500 \text{ kg/m}^3$ , a Bond albedo of 0.1, a thermal emissivity of 0.95, and a bulk density of  $3000 \text{ kg/m}^3$ . As our goal is to investigate the maximum possible diffusion of asteroids, we used two sets of spin axis orientations with  $\pm 90^\circ$  with respect to the orbital plane, since these obliquities maximize the speed of the Yarkovsky effect. We assumed periods obtained under the approximation that the rotation frequency is inversely proportional to the object’s radius, and that a 1 km asteroid had a rotation period of 5 hours

(Farinella et al. 1998)<sup>7</sup>. No re-orientations were considered, so that the drift caused by the Yarkovsky effect was the maximum possible.

We first performed “fast simulations” of these asteroids, assuming that all objects had 100 m diameters, over 30 Myr. Objects so small will drift much faster than the real asteroids, allowing for quicker simulations time-scales. On the other end, details of evolution in higher order mean-motion and secular resonances may be lost because of the faster drift. To account for this problem, we will also perform simulations with the real larger values of diameters “slow simulations”, scaled by factors  $\cos 30^\circ$  and  $\cos 60^\circ$  to account for values of the spin obliquity other than zero, that we will discuss later on in this section.

### 5.1 Results of the “fast simulations”

We obtained synthetic proper elements every 1.2 Myr for all the simulated asteroids with the approach described in Knežević and Milani (2003), modified as in Carruba (2010). Fig. 6 displays our results for asteroids in the Hansa region. Blue dots represent snapshots of the orbital evolution of clones of real asteroids with  $0^\circ$  obliquity, while yellow dots are associated with clones with  $180^\circ$  obliquity. The magenta lines display the chaotic layer near the 3J:-1A studied by Guillens et al. (2002), as defined in Morbidelli and Vokrouhlický (2003). The other symbols are the same as in Fig. 2.

One object near the Watsonia family was included in this region, having  $\sin(i) > 0.3$ , the criteria used by Gil-Hutton (2006) for identifying objects of high- $i$ . However, since its inclination is lower than the central value of the  $\nu_6$  secular resonance, other authors (Carruba 2010) may not consider this object a highly inclined body. The clone of the asteroid in the Gallia family region reached Mars crossing values of eccentricity when passing the 8J:-3A and was lost before the end of the simulation. One may notice that asteroids in the Hansa region are able to cross the 11J:-4A and 8J:-3A mean-motion resonances with only minor changes

<sup>7</sup> Other choices of rotation periods are possible. One can choose a distribution of rotation frequencies similar to that of other families, and randomly choose values for each asteroid. However, Cotto-Figueroa et al. (2013) have shown that the YORP effect is extremely sensitive to the topography of the asteroid, and its small changes. We therefore believe that in the end it may make little difference what initial rotation period is chosen. The rotation period of an asteroid will change during a YORP cycle in ways that are not currently well understood. Since our goal in this section is to preliminary investigate the fraction of surviving resonators when non-gravitational forces are considered, we believe that our simpler approach is justified.



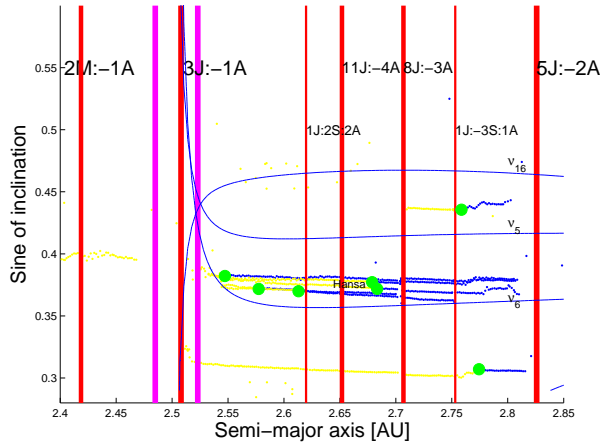


**Figure 6.** An  $(a, \sin(i))$  projection of the time evolution of fast clones or real V-type candidates in the Hansa region. Blue dots represent snapshots of the orbital evolution (sampled at each 1.2 Myr) of clones of real asteroids with  $0^\circ$  obliquity, while yellow dots are associated with clones with  $180^\circ$  obliquity. The other symbols are the same as in Fig. 2.

of inclination and reach the region of the Tina and Gallia families. Of particular interest was a clone with  $180^\circ$  obliquity, that succeeded in crossing the 3J:-1A mean-motion resonance. This suggests that evolution in the other direction may also be possible as suggested by Roig et al. (2008), and may have been responsible for the origin of the asteroids in the Hansa region, that may therefore be actual Vestoids, and originated from the inner main belt. A possible origin from the low-inclination central main belt seems unlikely, given the difficulties in crossing the dynamical boundary caused by the presence of the  $\nu_6$  secular resonance. Additional studies are needed on this subject to prove this hypothesis. Obtaining spectra of these asteroids and performing a comparative mineralogical analysis with respect to known Vestoids may provide important clues in understanding the origin of these objects.

In Fig. 7 we show the dynamical paths of clones of particles in the Eunomia region (panel A), and in the Gefion area (panel B). All three confirmed V-type asteroids in the central main belt are found in this region. Once again, we found particles (four) that manage to cross the main dynamical barriers of the 3J:-1A and 5J:-2A mean motion resonance, suggesting that small objects communication between inner and central main belt might be possible (how effective is this mechanism for larger asteroids will be discussed in Sect. 5.2). This could also have implication on the origin of V-type asteroids in the inner outer main belt (the area between the 5J:-2A and 9J:-4A mean-motion resonances with Jupiter), such as (10537) (1991 RY16), that could possibly be fragments of the parent body of the Merxia/Agnia families. Also, we found that most particles can easily cross the 11J:-4A and 8J:-3A mean-motion resonances, and that migration from the Eunomia region to the Gefion one (and vice-versa) is possible and could explain the presence of objects such (66905), as discussed in Carruba et al. (2007a). A few particles were captured in the secular resonances described in Sect. 4 and experienced moderate changes in in-

clinations. We did not however observed any particle able to reach the Astraea and Merxia regions in this simulation.

Fig. 8 displays the  $(a, \sin(i))$  projection of the time evolution of fast clones or real V-type candidates in the Astraea region (panel A) and in the Merxia region (panel B). One particle was able to cross the 3J:-1A mean-motion resonance and reached the region of low-inclination V-type asteroids in the inner main belt that Nesvorný et al. (2008) showed to be unlikely to originate from the current Vesta family. While this suggests that migration from the inner main belt into the central is possible, it may also open the possibility that the opposite happened, and that some of the low-inclination asteroids in the inner main belt may have originated from the central main belt, possibly from the parent body of the actual Merxia and Agnia families.

This seems to be supported by the fact that, once again, particles with 100 m diameter appear to be able to cross the 11J:-4A and 8J:-3A mean-motion resonances relatively unharmed. Communication from the Astraea region to the Merxia and vice-versa seems therefore, at least a possibility.

Finally, we also observed minor changes of inclination caused by secular resonances for some particles, but not enough to reach the Eunomia and Gefion regions. The possibility of migrations between the  $\sin(i) < 0.12$  and  $0.12 < \sin(i) < 0.3$  areas will be further investigated in the next subsection.

## 5.2 Results of the “slow simulations”

To further investigate the dynamical evolution of V-type candidates in the area, we performed “long-term” simulations of clones of the same particles studied in Sect. 5.1. These particles had the same parameters as in Sect. 5.1, except for the diameters and spin obliquities. We took the WISE values of the diameters for the test particles for which such information was available, and we used the methods described in Sect. 3 for the other particles. We also took six values of spin obliquities,  $0^\circ, 30^\circ, 60^\circ, 120^\circ, 150^\circ$ , and  $180^\circ$ , in order to sample different speeds of drifts caused by the Yarkovsky force. We integrated our test particles over 1 Byr, under the same integration scheme used in Sect. 5.1. Because of the longer integration time used in these runs, we computed proper elements every 4.9 Myr instead of the 1.2 Myr used in Sect. 5.1.

In the Hansa region, contrary to the case of the fast simulations, no particles managed to cross the 3J:-1A and 5J:-2A mean-motion resonances, nor any particles was able to cross the dynamical barrier of the  $\nu_6$  secular resonance. All particles that reached the 8J:-3A mean-motion resonance were able to cross over, and minor changes in sine of inclination, of up to 0.03, were observed after the passage of the 1J:-3S:1A three-body resonance. This suggests that the isolated V-type candidate in the Gallia family region could be explained by migration from the Hansa family region along with interaction with either the 8J:-3A or the 1J:-3S:1A mean-motion resonances. Possible source mechanisms for the Hansa family region V-type photometric candidates are still needed to explain the observed population of objects.

Similar results were observed for asteroids in the Eunomia, Gefion, and Merxia regions: no particle survived the crossing of the the 3J:-1A, 5J:-2A mean-motion resonances,

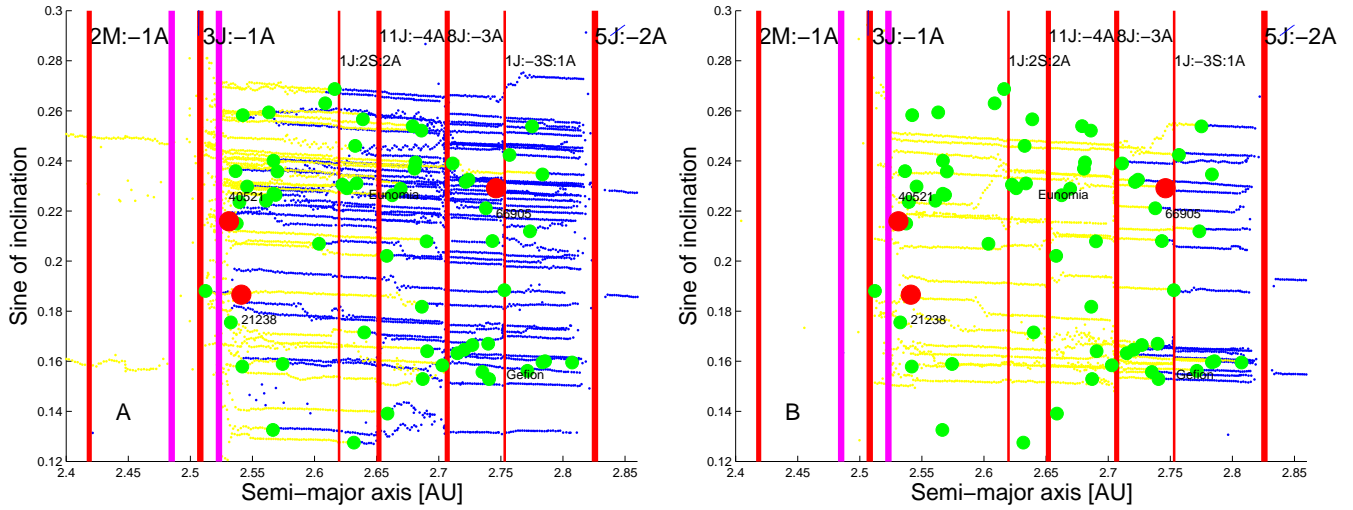


**Figure 7.** Panel A: An  $(a, \sin(i))$  projection of the time evolution of fast clones or real V-type candidates in the Eunomia region. Panel B: the same for clones of asteroids in the Gefion region. See caption of Fig. 6 for a description of the used symbols.

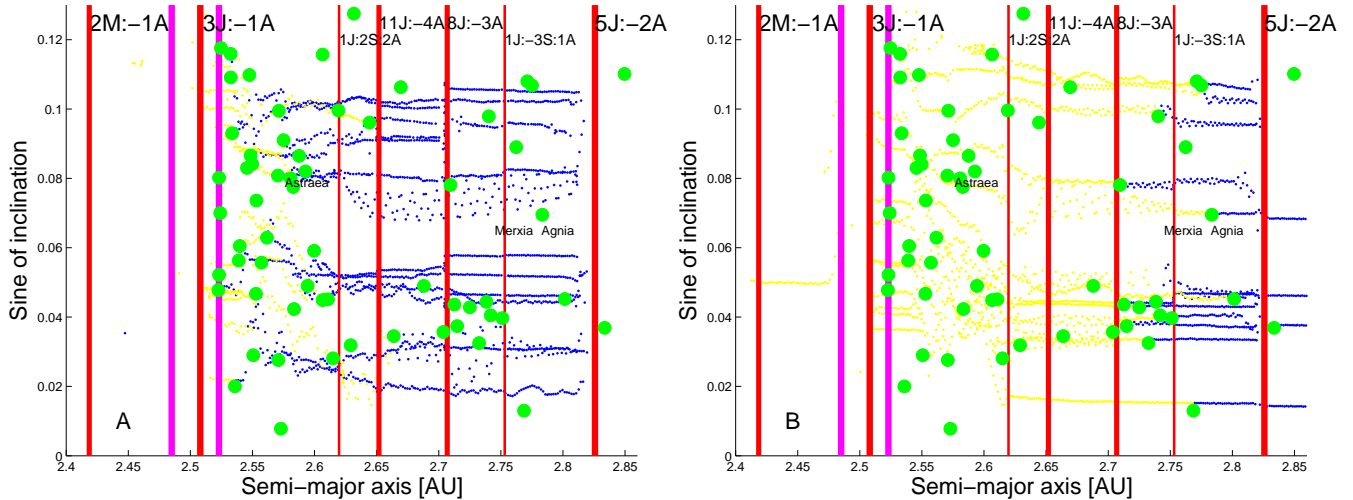


**Figure 8.** Panel A: An  $(a, \sin(i))$  projection of the time evolution of fast clones or real V-type candidates in the Astraea region. Panel B: the same for clones of asteroids in the Merxia region. See caption of Fig. 6 for a description of the used symbols.

and no particle managed to pass the  $\nu_6$  secular resonance barrier. At least 80% of the asteroids that reached the 8J:-3A and the 1J:-3S:1A mean-motion resonance were able to cross over. Changes in inclination of up to 0.3 in  $\sin i$  caused by interactions with the  $2\nu_6 - \nu_5$  secular resonances were also observed in the Eunomia region, but this was not enough to allow particles to change region (as changes occurred for values of increasing  $i$ , i.e., in the opposite direction to reach the Astraea region). We did not observe any particle changing regions in inclination during the length of our simulations.

Results were more interesting in the Astraea region. As discussed in Sect. 4, particles in this region strongly interacted with the  $2\nu_6 - \nu_5$  non-linear secular resonance, and this results in large oscillations of  $\sin(i)$  values. Several particles are attracted by this powerful resonance, creating a “convergence zone” of V-type photometric candidates, roughly

located between the 3J:-1A and 11J:-4A mean-motion resonances in semi-major axis (see also Fig. 4 and the yellow dots associated with the same resonance for a better definition of this region), and also shown in Fig. 9, that displays the time evolution in the  $(a, \sin(i))$  plane of clones of V-type candidates with obliquities of  $0^\circ$  and  $180^\circ$ . Yet, oscillations are limited to the Astraea region. Only one particle managed to evolve in the  $2\nu_6 - \nu_5$  to higher values of inclinations, but it was soon lost because of its interaction with the 3J:-1A mean-motion resonance. No particle managed to cross the 3J:-1A and survive in the inner main belt for more than 10 Myr.

Overall, our simulations seem to confirm our hypothesis of a bimodal source for V-type asteroids in the central main belt, with the parent bodies of the Eunomia family and of the Merxia and Agnia ones as possible sources. The

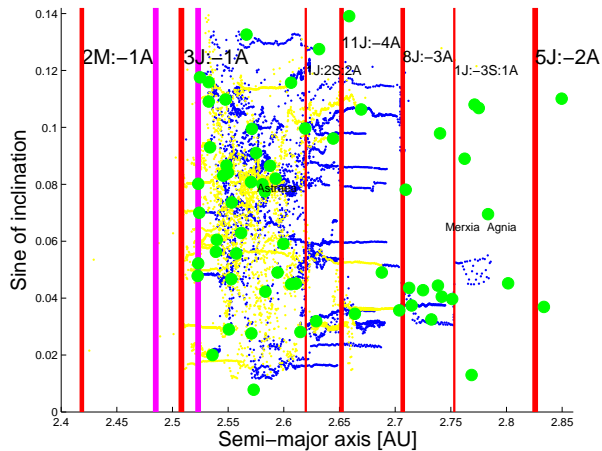


**Figure 9.** An  $(a, \sin(i))$  projection of the time evolution of slow clones or real V-type candidates in the Astraea region. See caption of Fig. 6 for a description of the used symbols.

fact that no particle, during our simulations, switched in a stable fashion among inclination regions does not exclude that such orbital evolution is possible, but suggests, in our opinion, that these should be a rare event. To investigate if dynamical mobility caused by other mechanisms such as close encounters with massive asteroids could account for such dynamics, we will present results of new simulations that also account for this mechanism in the next section.

## 6 EFFECTS OF CLOSE ENCOUNTERS WITH MASSIVE ASTEROIDS

In order to investigate the effects of close encounters with massive asteroids we integrated all V-type photometric candidates over the gravitational influence of all planets plus Ceres, Eunomia, and Juno, the most massive asteroids in the central main belt and some of the most effective perturbers (see Carruba et al. (2013a) for a list of the first 40 most massive asteroids in the main belt), over 200 Myr. We did not include the effect of Pallas, since Carruba et al. (2013a) showed that the long-term effect of close encounters with this asteroid is less significant than that of other, less inclined bodies, such as Ceres or Hygiea, and we also did not simulate the Yarkovsky effect. Since our goal was to obtain a complete statistics of change in orbital elements due to close encounters, and since this statistics does not strongly depend on the model used (Carruba et al. 2012), we simply used SWIFT-SKEEL, the integrator of the SyMBA package able to simulate close encounters among massive planets and massless particles (Levison and Duncan 1994), without attempting to include non-gravitational effects, and with the simulation set-up discussed in Carruba et al. (2013a).

In this work we were mostly interested in dynamical mobility in inclination, because these are the changes that can cause an asteroid to switch zones, so “contaminating” one source of basaltic material with another. Obtaining changes in proper inclination caused by close encounters only is not a straightforward task. That could be accomplished by obtaining proper elements before and after the encounter, and

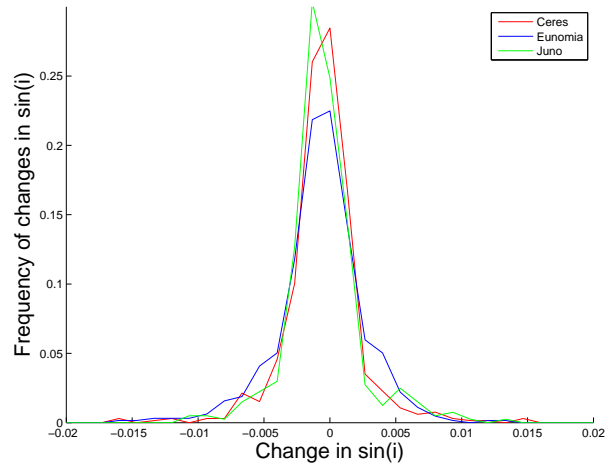


**Figure 10.** Frequencies of changes in osculating  $\sin(i)$  caused by close encounters with (1) Ceres (red line), (15) Eunomia (blue line), and (3) Juno (green line).

by trying to isolate contributions to the changes in proper  $i$  other than the close encounter (passage through mean-motion resonances, secular effects, etc.). As a first step in our analysis, we just computed changes in osculating  $\sin(i)$ , in order to have a preliminary estimate of the entity of possible changes in proper  $i$ .

Our results are shown in Fig. 10, where the red line identifies the frequency distribution of changes in  $\sin(i)$  caused by encounters with (1) Ceres, the blue line those caused by (15) Eunomia, and the green line those caused by (3) Juno. During our simulations we registered 657 encounters with Ceres, 636 with Eunomia, and 402 with Juno, which, according to Carruba et al. (2013a), should be enough to obtain a statistics complete to a  $1\sigma$  level, sufficient to start an analysis of the long-term effect of close encounters. As expected, most of the encounters cause a limited change in  $\sin(i)$ , with less than 1% of the encounters causing larger variations (the percentage is higher for Ceres being this the most massive body). Larger variations, corresponding to encounters at very close relative distances or velocities, are possible, but are very rare events. Also, in order to allow for an asteroid to switch zones in inclination, they should happen repeatedly and in the “right” direction (to lower inclinations for Eunomia region asteroids and to higher for Astraea region ones).

In order to have a preliminary quantitative estimate of the long term effect of close encounters with massive asteroids we assume in first approximation that such mechanism could be treated as a random walk. Under the assumption, as it seems to be the case for our observed distributions of changes in  $\sin(i)$ , that the mean value of changes is zero, there will be a  $1\sigma$  ( $= 68.27\%$ ) probability that the root mean square translation distance (or quadratic mean) after  $n$  steps will fall between  $\pm\sigma_{\sin(i)}\sqrt{n}$ , where  $\sigma_{\sin(i)}$  is the standard deviation of changes in  $\sin(i)$ , equal to 0.0029 for the distribution of changes in  $i$  caused by (1) Ceres, by far the main perturber in the central main belt (Carruba et al. 2003, 2013a). Since Bottke et al. (2006) estimated that the parent bodies of differentiated objects arrived in the main belt no earlier than 4 Byr ago, using the value of

$\sigma_{\sin(i)}$  obtained for changes in  $\sin(i)$  caused by (1) Ceres over 200 Myr, and  $n = 20$ , we obtained a root mean square translation of 0.0130. Considering our boundary between inclination regions at  $\sin(i) = 0.12$ , only 9 objects (7 in the Merxia/Agnia and 2 in the Eunomia region) are in the region  $0.12 \pm \sigma_{\sin(i)}\sqrt{n}$  and could therefore experience a change in  $\sin(i)$  large enough to allow for a change of region over 4 Byr, at  $1\sigma$  level of probability, i.e., 7% of the total.

Close encounters with massive asteroids may have allowed for some mixing between asteroids from the Eunomia and the Merxia/Agnia regions, but a single source mechanism seems to be statistically unlikely.

## 7 CONCLUSIONS

In this work we:

- Revised the current knowledge on V-type photometric candidates (Carvano et al. 2010) and obtained new photometric candidates with the approach of DeMeo and Carry (2013). Overall, we identified 127 V-type photometric candidates in the central main belt, six of which belong to the Eunomia family, and four of which are Hansa family members.

- Obtained distances with respect to (15) Eunomia and (808) Merxia for all V-type photometric candidates, using the distance metrics of Zappalá et al. (1995). Three regions in inclination appear using this approach, suggesting a three-source model for the origin of V-type asteroids in the central main belt: highly-inclined asteroids above the  $\nu_6$  secular resonance (Hansa region), asteroids with  $0.12 < \sin(i) < 0.3$  (Eunomia region), and asteroids with  $\sin(i) < 0.12$  (Astraea region). Additional subdivision can be set by considering the presence of the 8J:-3A mean-motion resonance (Gefion region in the Eunomia region, and Merxia region in the Astraea region).

- Obtained a synthetic proper element dynamical map of the central main belt in the proper  $(a, \sin(i))$  plane for 19800 test particles, and studied mean-motion and secular resonances (up to order six) in the region. As hypothesized in Carruba et al. (2007a), the  $\nu_5 - \nu + \nu_{16}$  could be a viable mechanism to reduce asteroids inclinations, but only for asteroids in the Eunomia region, and not to values of  $i$  in the Astraea region range. 15 V-type photometric candidates are currently in librating states of the  $2\nu_6 - \nu_5$  secular resonance, and the local increase in number of these bodies in the Astraea region could therefore be an artifact of the local dynamics.

- Studied the Yarkovsky-induced dynamical evolution of clones of all V-type photometric candidates. Our simulations suggest that the current orbital distribution of these objects could be explained with a two sources mechanism originating in the parent bodies of the Eunomia and Agnia/Merxia families (with a third possible source in the parent body of the Hansa family). With one (unstable) exception, no particle during our simulation managed to switch among inclination regions, and no particles with diameters larger than 1 km succeeded in crossing the 3J:-1A mean-motion resonance barrier, suggesting that asteroids from the Vesta family should be rare among central V-type photometric candidates.
- Studied the effects of close encounters with (1) Ceres,

(15) Eunomia, and (3) Juno for the V-type photometric candidates. Only less than 1% of the studied encounters caused a change in osculating  $\sin(i)$  larger than 0.01 in module, and no particle changed inclination zones over the length of our integrations. We estimated that, at  $1\sigma$  level probability, at most 7.0% of the known V-type photometric candidates could have changed inclination region over 4 Byr.

Many new basaltic candidates have been identified since the three originally suggested in 2007 (see also Carruba et al 2007a for a review on V-type asteroids in the central main belt known at that time), and this allowed us to perform a more in depth analysis of their possible origin. Many more other asteroids may be missing or unobservable either because comminuted to sizes below observational limits (Burbine et al. 1996), or because of space weathering effects that obscured the basaltic signature in their spectra (Wetherill and Chapman, 1988).

For the currently known V-type candidates, we showed that a two source scenario, the parent bodies of the Eunomia plus Merxia and Agnia families, could explain the origin of most of the basaltic material in the central main belt, with a fraction that may come from other sources (either from the inner main belt, diffusing across the 3J:-1A mean-motion resonance (Roig et al. 2008), or because of some unusual mechanism of scattering, such very close encounters with massive asteroids, able to increase the inclination of an object above the values of the center of the  $\nu_6$  secular resonance<sup>8</sup>). According to Bottke et al. (2006), the parent bodies of V-type asteroids in the central main belt could possibly have been formed much closer than their current orbital location, in the terrestrial planet region, and then have been scattered by close encounters with planetesimals in the early phase of the Solar System formation, 4.0 Gyr ago or more. Considering that the number of scattered differentiated bodies is model dependent and ranges from one to several hundreds in Bottke et al. (2006) theory, depending on the region of formation of differentiated bodies and on the minimum value of diameter needed to insure differentiation, we believe that a scenario in which two or three differentiated bodies were injected into the central main belt and then disrupted by collisions could explain the current observed distribution of V-type photometric candidates in the central main belt<sup>9</sup>.

In this framework, it is of utmost importance to conduct a mineralogical analysis of the V-type candidates studied in this work. Sunshine et al. (2004) showed that Vestoids have much deeper band depths than the HCP-rich S-type asteroids. This could be used to discriminate the asteroids in the Astraea region that originated from Vesta from those that originated from the parent body of the Agnia and Merxia families, and could be also important in assessing the origin of the highly inclined V-type objects whose origin cannot be easily explained with scenarios involving central main belt

<sup>8</sup> Highly inclined V-type photometric candidates could also be explained under the assumption of a third local source of basaltic material, if we assume that the parent body of the Hansa family was a differentiated or partially differentiated asteroid.

<sup>9</sup> Alternatively, depending on the parameters of Bottke's theory, one could also imagine that all central main belt V-type candidates were scattered from the terrestrial planet region.

sources. Overall, a lot of work remains to be done to understand the origin and the dynamical evolution of V-type asteroids in the central main belt.

## ACKNOWLEDGMENTS

We are grateful to the reviewer of this article, Nicholas Moskowicz, for suggestions and comments that significantly improved the quality of this work. We would like to thank the São Paulo State Science Foundation (FAPESP) that supported this work via the grant 11/19863-3, and the Brazilian National Research Council (CNPq, grant 305453/2011-4). This publication makes use of data products from the Wide-field Infrared Survey Explorer, which is a joint project of the University of California, Los Angeles, and the Jet Propulsion Laboratory/California Institute of Technology, funded by the National Aeronautics and Space Administration. This publication also makes use of data products from NEOWISE, which is a project of the Jet Propulsion Laboratory/California Institute of Technology, funded by the Planetary Science Division of the National Aeronautics and Space Administration.

## 8 APPENDIX

Table 3 reports the asteroid identification, its proper  $a$ ,  $e$ , and  $\sin(i)$ , its absolute magnitude ( $H$ ), diameter ( $D$ ), and geometric albedo ( $p_V$ ), according to the WISE mission, when available, for all asteroids in the central main belt identified in Carvano et al. (2010). Asteroids without WISE data on  $D$  and  $p_V$  have been assigned the mean value of geometric albedo of V-type asteroids in the central main belt, and diameters computed according to Eq. 8 (for simplicity, we do not report these data in the Table). For asteroids likely to be in a secular resonance configuration, we also report the resonance name. Finally, we specified the region to which the asteroid belongs to, according to the classification scheme of Sect. 2, and listed asteroids accordingly.

Table 3: List of V-type photometric candidates in the central Main-Belt

Asteroid id.	$a$	$e$	$\sin(i)$	H	D (km)	$p_v$	Seculare resonance name
<b>Hansa region</b>							
44257	2.5472	0.0392	0.3822	13.70	4.6450	0.2710	
62002	2.7586	0.2264	0.4356	14.90			
87908	2.6833	0.0552	0.3718	14.10	3.8760	0.2456	
118748	2.6130	0.0763	0.3699	16.90			
122662	2.5774	0.0674	0.3717	15.00	3.0520	0.2741	
182339	2.6788	0.0338	0.3772	15.79			
217433	2.7743	0.0840	0.3071	14.97			$3\nu_6 - \nu_5$
<b>Eunomia region</b>							
21238	2.5411	0.1371	0.1866	12.90	5.2210	0.3729	
24014	2.5609	0.1709	0.2241	13.10	6.5670	0.2357	
40521	2.5311	0.0458	0.2159	14.90	2.6370	0.2785	
44447	2.5701	0.1641	0.2358	14.70	3.7360	0.1668	$3\nu_6 - \nu_5$
55550	2.5457	0.1444	0.2298	15.30			
56904	2.6338	0.1733	0.2310	14.90			$2\nu_6 + \nu_{16} = z_2$
81147	2.5326	0.0927	0.1755	15.00			$\nu_6 + \nu_{16} = z_1$
84021	2.6790	0.0911	0.2539	15.40			$3\nu_6 - \nu_5$
88533	2.6581	0.1374	0.2021	15.10			
90649	2.6587	0.1606	0.1391	15.80			
93620	2.6327	0.1437	0.2460	14.70	2.5870	0.3173	$3\nu_6 - \nu_5, 2\nu_6 + \nu_{16} = z_2$
108139	2.5374	0.2553	0.2150	14.90	3.3020	0.1777	
110998	2.6162	0.0392	0.2687	15.00			
120236	2.6086	0.1994	0.2630	16.90			
126729	2.6389	0.1217	0.2566	15.60	2.1150	0.2272	
147640	2.5686	0.1568	0.2264	15.30			
170007	2.6907	0.1364	0.1640	16.60			
170015	2.6871	0.2185	0.1529	15.80			$2\nu_6 - \nu_5$
189759	2.5743	0.0483	0.1589	15.47			
196445	2.5418	0.1995	0.1579	16.15			
196484	2.5665	0.1712	0.1326	16.27			
201693	2.5669	0.0534	0.2401	15.69			
202118	2.5364	0.0713	0.2359	16.14			
203669	2.5422	0.1875	0.2583	15.51	1.7190	0.3441	
208783	2.5395	0.2659	0.2236	15.60	2.4620	0.1676	
238208	2.7029	0.0674	0.1584	16.15	2.2480	0.1269	
239099	2.6036	0.0754	0.2069	16.19			
242039	2.6864	0.0525	0.1818	15.69			
243029	2.6860	0.0776	0.2521	15.67	2.4220	0.1580	
249831	2.6400	0.1598	0.1715	15.84			
262637	2.6259	0.2339	0.2291	16.20			
271071	2.5631	0.0878	0.2594	15.74			
275687	2.5668	0.1438	0.2269	16.67			
279983	2.6813	0.0669	0.2394	16.24			
302936	2.5122	0.1003	0.1881	16.63			
318027	2.6694	0.2368	0.2289	16.54			
324579	2.6805	0.0786	0.2369	16.60			
341273	2.7835	0.0530	0.2346	15.74			
363180	2.6317	0.1740	0.1275	16.78			
363846	2.6225	0.1295	0.2305	16.06			
367188	2.6902	0.0257	0.2079	15.90			
<b>Astraea region</b>							
22893	2.5326	0.1893	0.1091	15.10			
29720	2.6638	0.0846	0.0345	15.30			$\nu_6 + \nu_{16} = z_1$
46626	2.5359	0.1602	0.0200	14.60			
57439	2.5617	0.0677	0.0629	15.40			
58424	2.5337	0.1850	0.0930	15.50			

*Continued on next page*

Table 3 – Continued from previous page

Asteroid id.	$a$	$e$	$\sin(i)$	H	D (km)	$p_v$	Secular resonance name
67299	2.5751	0.2692	0.0910	14.90			
68635	2.5808	0.2461	0.0800	16.30	2.0110	0.3633	
89387	2.5507	0.1417	0.0290	16.00			
93580	2.6443	0.2865	0.0961	16.70			
102973	2.6108	0.1347	0.0451	15.90			
108901	2.5944	0.1206	0.0490	16.60			$2\nu_6 - \nu_5, \nu_6 + \nu_{16} = z_1$
119360	2.5498	0.1403	0.0841	16.60			$2\nu_6 - \nu_5$
121046	2.5226	0.1289	0.0478	16.70			
122758	2.5705	0.1892	0.0808	17.20			$2\nu_6 - \nu_5$
123441	2.6291	0.0710	0.0319	16.30			
127242	2.5398	0.1603	0.0605	15.70	2.0490	0.2014	
129632	2.5325	0.2441	0.1159	16.20	1.5120	0.3373	
129633	2.5231	0.1693	0.0802	16.30			
134783	2.6065	0.0105	0.0449	16.30			$2\nu_6 - \nu_5$
136823	2.6192	0.2200	0.0996	16.20			$2\nu_6 - \nu_5$
137139	2.5456	0.2783	0.0830	16.20			
138114	2.5476	0.2404	0.1098	16.80			
148699	2.6695	0.1238	0.1063	16.10			
149588	2.5390	0.0699	0.0563	16.50			
152062	2.5713	0.2847	0.0995	16.40			
154704	2.5528	0.1659	0.0467	16.50			
158290	2.5709	0.1111	0.0276	17.00			$2\nu_6 - \nu_5$
160623	2.6065	0.1961	0.1157	15.80			
161465	2.7037	0.0624	0.0357	15.80			
177717	2.5485	0.0615	0.0866	15.91			
181565	2.6149	0.1103	0.0281	16.40			
187458	2.5927	0.1854	0.0820	15.14			$2\nu_6 - \nu_5$
189410	2.5876	0.2541	0.0865	14.64			$2\nu_6 - \nu_5$
225791	2.5835	0.1124	0.0423	17.22			$2\nu_6 - \nu_5, 2\nu_6 + \nu_{17}$
240369	2.5241	0.0551	0.0700	16.58			
271802	2.6880	0.0836	0.0490	17.42			
287090	2.5247	0.2083	0.1176	17.68			
293407	2.5829	0.1698	0.0775	17.42			$2\nu_6 - \nu_5$
327872	2.5996	0.1696	0.0591	17.17			
329973	2.5729	0.0895	0.0078	17.57			$2\nu_6 - \nu_5$
366838	2.5532	0.2321	0.0736	18.11			
370092	2.5231	0.2077	0.0522	17.74			
370122	2.5573	0.1022	0.0557	17.44			
<b>Gefion Region</b>							
7302	2.8074	0.1468	0.1595	12.10	10.6290	0.2082	
22308	2.7734	0.1126	0.2119	14.00	5.8230	0.1573	
37325	2.7398	0.1831	0.1670	14.30			
66905	2.7462	0.1458	0.2291	15.30			
87110	2.7112	0.1606	0.2390	15.00			
93322	2.7432	0.0990	0.2080	15.30	3.2540	0.1829	
104359	2.7714	0.1360	0.1562	15.10			
113194	2.7206	0.1037	0.1646	15.30			$2\nu_6 - \nu_5$
119686	2.7150	0.1796	0.1632	15.30			$2\nu_6 - \nu_5$
126955	2.7352	0.1396	0.1557	15.00			
133990	2.7751	0.0255	0.2538	15.50			
150512	2.7216	0.1042	0.2316	15.90			
179216	2.7529	0.0648	0.1884	15.61			
182385	2.7271	0.1809	0.1665	15.00	1.8520	0.2464	$2\nu_6 - \nu_5$
186607	2.7570	0.0659	0.2424	15.25			
202242	2.7379	0.1596	0.2211	15.28	2.2360	0.2230	
206011	2.7240	0.0334	0.2325	15.42	2.4360	0.1713	$\nu_5 - \nu_6 + \nu_{16}$
233474	2.7835	0.1218	0.1596	15.91			

Continued on next page

Table 3 – *Continued from previous page*

Asteroid id.	$a$	$e$	$\sin(i)$	H	D (km)	$p_v$	Secular resonance name
258311	2.7856	0.0858	0.1600	16.26			$2\nu_6 + \nu_{17}$
340344	2.7405	0.1311	0.1529	16.99			
<b>Merxia region</b>							
36118	2.7095	0.0742	0.0781	13.40	4.9980	0.3385	
36590	2.8336	0.0473	0.0369	15.40	2.7020	0.1674	
48558	2.7624	0.1386	0.0890	15.40			
85402	2.7325	0.0577	0.0325	15.00			
88727	2.8015	0.1192	0.0452	15.00			
88754	2.7384	0.0744	0.0444	14.90			$\nu_6 + \nu_{16} = z_1$
95536	2.7512	0.1011	0.0397	15.90			
155236	2.7148	0.0620	0.0374	16.20			
171403	2.7834	0.0504	0.0695	15.80			
126639	2.7250	0.0401	0.0428	15.80			
208899	2.7751	0.0392	0.1068	15.73			
209318	2.7403	0.0419	0.0979	16.78			
233503	2.7126	0.0323	0.0436	16.06			
243256	2.7713	0.0901	0.1080	16.05	3.5200	0.0518	
289970	2.7687	0.0494	0.0130	16.86			
348518	2.7419	0.0538	0.0405	16.86			



## REFERENCES

- Bottke, W. F., Nesvorný, D., Grimm, R. E., Morbidelli, A., O'Brien, D. P., 2006, *Nature*, 439, 821.
- Brož, M., 1999, Thesis, Charles Univ., Prague, Czech Republic.
- Burbine, T. H., Meibom, A. Binzel, R. P., *Met. & Planet. Sci.* 31. 607.
- Carruba V., Burns, J. A., Bottke, W., Nesvorný, D. 2003, *Icarus*, 162, 308.
- Carruba, V., Michtchenko, T., Lazzaro, D., 2007a, *A&A*, 473, 967.
- Carruba, V., Michtchenko, T., 2007b, *A&A*, 475, 1145.
- Carruba, V., Michtchenko, T., 2009, *A&A*, 493, 267.
- Carruba, V., 2009a, *MNRAS*, 395, 358
- Carruba, V., 2010, *MNRAS*, 408, 580.
- Carruba, V., Machuca, J. F., 2011, *MNRAS*, 420, 1779.
- Carruba, V. Huaman, M. E., Douwens, S., Domingos, 2012, *A&A*, 543, A105.
- Carruba, V. Huaman, M. E., Domingos, R. Roig, F. 2013a, *A&A*, 550, A85.
- Carruba, V. Domingos, R. C., Huaman, Dos Santos, C. R., Souami, D., 2013b, *MNRAS*, 433, 2075.
- Carvano, J. M., Hasselmann, P. H., Lazzaro, D., Mothé-Diniz, T., 2010, *A&A*, 510, A43.
- Cotto-Figueroa, D., Statler, T. S., Richardson, D. C., Tanga, P. 2013, *DDA*, 102.02.
- DeMeo, F., Carry, B. 2013, *Icarus*, 266, 723.
- DeSanctis M. C., Ammannito, E., Migliorini, A., Lazzaro, D., Capria, M., T., McFadden, L. 2011, *MNRAS*, 412, 2318.
- Farinella, P., Vokrouhlický, D., Hartmann, W. K., 1998, *Icarus*, 132, 378.
- Gil-Hutton, R., 2006, *Icarus*, 183, 93.
- Guillens, S. A., Vieira Martins, R., Gomes, R. S. 2002, *AJ*, 124, 2322.
- Harris, A. W., Lagerros, J. S. V., 2002, *Asteroids III*, W. F. Bottke Jr., A. Cellino, P. Paolicchi, and R. P. Binzel (eds), University of Arizona Press, Tucson, 205-218.
- Ivezić, Ž, and 32 co-authors, 2001, *AJ*, 122, 2749.
- Knežević, Z., Milani, A., 2003, *A&A*, 403, 1165.
- Lazzaro, D., and 10 co-authors, 2000, *Science*, 288, 2033.
- Levison, H. F., Duncan, M. J., 1994, *Icarus*, 108, 18.
- Masiero, J. R., and 17 co-authors, *ApJ* 741, 68.
- Mainzer, A. K., and 34 co-authors, 2011, *ApJ* 731, 53.
- Mardia, K., V., 1970, *Biometrika* 57, 519.
- Masiero, J. R., and 17 co-authors, 2011, *ApJ* 741, 68.
- Milani, A., Knežević, Z. *Icarus*, 1994, 107. 219.
- Morbidelli A., Vokrouhlický, D., 2003, *Icarus* 163, 120.
- Moskovitz, N. A., and six co-authors 2008a, *Icarus* 198, 77.
- Moskovitz, N. A. and six co-authors 2008b, *AJ* 682, 57.
- Nathues, A., Mottola, S., Kaasalainen, M., Neukum, G., 2005, *Icarus*, 175, 452.
- Nesvorný, D., and 5 co-authors, 2008, *Icarus*, 193, 85.
- Roig F., Gil-Hutton R., 2006, *Icarus*, 183, 411.
- Roig F., Nesvorný, D. Gil-Hutton R., Lazzaro, D., 2008, *Icarus*, 194, 125.
- Sunshine, J. and five co-authors, 2004, *Meteorit. Planet. Sci.* 39, 1343.
- Vokrouhlický D., Brož, M., Bottke, W. F., Nesvorný, D., Morbidelli, A. 2006, *Icarus*, 183, 349.
- Wetherill, G. W., Chapman, C. R., 1988, *Asteroids and Meteorites*. In Kerridge, J. F., Matthews, M. S., (Eds), *Meteorites and the Early Solar System*, Univ. of Arizona Press, Tucson, 35.
- Wright, E. L., and 37 co-authors, 2010, *AJ*, 140, 1868.
- Zappalà, V., Bendjoya, Ph., Cellino, A., Farinella, P., Froeschlé, C., 1995, *Icarus*, 116, 291.

This paper has been typeset from a  $\text{T}_{\text{E}}\text{X}/\text{L}^{\text{A}}\text{T}_{\text{E}}\text{X}$  file prepared by the author.

